Key temperature-dependent characteristics of AlGaN-based UV-C laser diode and demonstration of room-temperature continuous-wave lasing

Ziyi Zhang,[1,2,a)] Maki Kushimoto,[3] Akira Yoshikawa,[1,2] Koji Aoto,[1,4] Chiaki Sasaoka,[4] Leo J. Schowalter,[4] and Hiroshi Amano[4]

[1)]*Advanced Devices Technology Center, Corporate Research & Development, Asahi Kasei Corporation, Chiyoda, Tokyo 100-0006, Japan*

[2)]*Center for Integrated Research of Future Electronics, Institute of Materials Research and System for Sustainability, Nagoya University, Chikusa, Aichi 464-8601, Japan*

[3)]*Graduate School of Engineering, Nagoya University, Chikusa, Nagoya, Aichi 464-8603, Japan*

[4)]*Center for Integrated Research of Future Electronics, Institute of Materials Research and System for Sustainability, Nagoya University, Chikusa, Nagoya, Aichi 464-8601, Japan*

(Dated: 28 September 2022)

Although the pulsed operation of AlGaN-based laser diodes at UV-C wavelengths has been confirmed in previous studies, continuous oscillation without cooling is difficult because of the high operating voltage. In this study, the temperature dependence of key parameters was investigated and their impact on achieving continuous-wave lasing was discussed. A reduction in threshold voltage was achieved by tapering the sides of the laser diode mesa and reducing the lateral distance between the n- and p-electrodes. As a result, continuous-wave lasing at room temperature was demonstrated for the first time at a threshold current density of $4.2\,\mathrm{kA/cm^2}$ and a threshold voltage of 8.7 V.

Semiconductor ultraviolet laser diodes (LDs) with wavelengths shorter than 280 nm (so-called UV-C LDs) have long been desired for instrumentation applications[1–4], specialty laser machining[5,6], and even improved disinfection applications[7]. However, even though such lasers were first demonstrated[8], efficiency and lifetime must still be substantially improved before practical applications can be realized. The initial demonstration of LDs only allowed pulsed operation and, while recent progress showed that continuous-wave (CW) operation was possible, it was only achieved with operation below room temperature[9]. In this paper, we present a detailed discussion of the effects of temperature on UV-C LDs. While the series resistance of the diodes shows relatively little temperature dependence, the threshold current varies substantially with temperature and can be described with a characteristic temperature of 70 K. By understanding the temperature characteristics, it became possible to quantitatively discuss how the increase in junction temperature owing to self-heating during DC drive inhibits CW operation. The room-temperature CW lasing of fully packaged UV-C LD is demonstrated for the first time by improving the device design to lower the junction temperature when the LD is operated above the threshold current.

In the present work, an AlGaN-based UV-C LD structure was grown pseudomorphically on the (0001) (Al-polar) face of 2-inch, single-crystal AlN substrates[10] by MOCVD. The structure consisted of a 400-nm-thick, Si-doped $Al_{0.75}Ga_{0.25}N$ n-cladding layer, a 120-nm-thick undoped $Al_{0.63}Ga_{0.37}N$ waveguide layer that included an active layer consisting of two 4.5-nm-thick quantum wells, a 320-nm-thick p-type distributed polarization doped (p-DPD) cladding layer and a 50-nm-thick p-contact layer including an additional Al compositionally graded layer capped with Mg-doped GaN. The Al composition x of $Al_xGa_{1-x}N$ was decreased from 1.0 to 0.7 in the growth direction of the p-DPD cladding layer without any intentional impurity doping. The AlGaN layers were confirmed to be fully strained to the AlN substrate by $(10\bar{1}5)$ X-ray reciprocal space mapping. The epitaxial layer was then fabricated into LD chips with a resonator length of $600\,\mu\mathrm{m}$ and a p-electrode width of $5\,\mu\mathrm{m}$. The shape of the mesa edges were carefully controlled to be a 15° slope to the (0001) surface. This angle was sufficiently shallow to effectively suppress dislocation formation that can result from the concentrated shear stress generated at the mesa edge. Since these shear-stress-generated dislocations significantly deteriorate the active layer near the mesa edge, the p-electrode must be placed further from the mesa edge in the previous studies[11]. By suppressing the dislocation formation using the sloped-mesa technique, the p-electrode now can be placed closer to the mesa edge (also the n-electrode) so that the distance the current must pass through the n-cladding layer is shortened and the series resistance of the device could be reduced. Cleaved facets with high-reflection coatings (reflectivity above 0.9) were used at both ends of the LD. The fabricated chips were then packaged in a 5.6 mm TO-CAN that included wiring to the p-electrode and to both n-electrodes on each side of the mesa. A schematic drawing of the fabricated LD chip is shown in Fig. 1. A cross-sectional SEM image of mesa edge is also shown.

The temperature dependences of light–current–voltage (L–I–V) characteristics of a fully packaged device were measured using a Perlite thermostage between −5 and 65 °C. Thermal grease was used to improve the thermal contact between the device package and the copper stage while short pulses and a very low duty cycle (100 ns and 0.02%, respectively) were used to prevent the heating of the LD junction above the stage temperature during pulsed operation. A calibrated Si photodiode was used to measure the edge-emission optical power. The measured L–I–V characteristics and the threshold current

[a)]Electronic mail: zhang.zc@om.asahi-kasei.co.jp

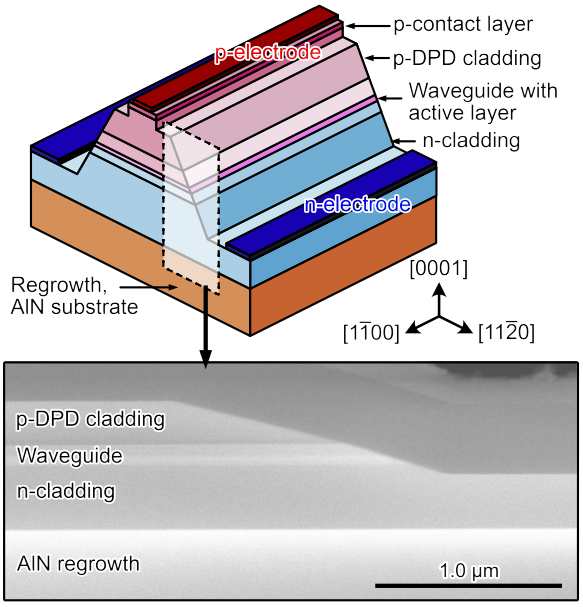

FIG. 1. Schematic drawing of fabricated UV-C LD structure and cross-sectional SEM image of sloped mesa edge.

dependence on the temperature are shown in Fig. 2. The temperature dependence of the threshold current $I_{th,p}$ was fitted using

$$I_{th,p}(\Delta T) = I_{th,p}^{RT} \exp\left(\frac{\Delta T}{T_0}\right) \quad (1)$$

to extract the characteristic temperature T_0 of 70 K. Here, $I_{th,p}^{RT}$ represents the threshold current with pulse drive at room temperature (298 K) and ΔT represents the deviation of the junction temperature from room temperature. The series resistance R_s extracted at currents above $I_{th,p}$ was 8.4 Ω and was almost constant over the measured temperature range. Emission spectra were measured over the temperature range in 10 °C steps at drive currents slightly above the threshold ($1.1 \times I_{th,p}$) for that particular temperature. The peak wavelength λ_p was 274 nm at room temperature, and its shift with temperature ($d\lambda_p/dT$) was found to be 32 pm/K.

Finally, the L–I–V characteristics were measured at room temperature (without stage temperature control) under direct current operation and compared with those measured under pulsed current operation, as shown in Fig. 4. CW lasing was successfully achieved at driving currents above $I_{th,c}$ = 125 mA, which corresponds to 4.2 kA/cm^2 assuming uniform current injection from the p-electrode. The threshold operating voltage $V_{th,c}$ at the threshold current was 8.7 V. The horizontal and vertical far-field patterns (FFP) were also characterized under pulsed operation at peak output power of 1 mW, as shown in Fig. 5. As shown in Fig. 5, multiple peaks were found in the horizontal FFP. This suggests that multiple transverse modes are allowed, consistent with the fact that no attempt was made to achieve single transverse mode confinement in the current design. The full-widths at half-maximum

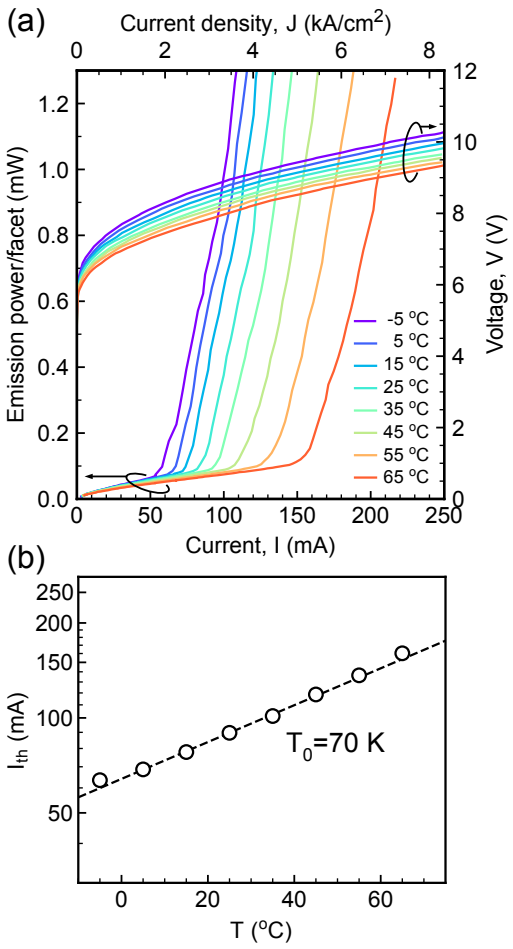

FIG. 2. (a) Temperature-dependent L–I–V characteristics under pulse operation and (b) threshold current.

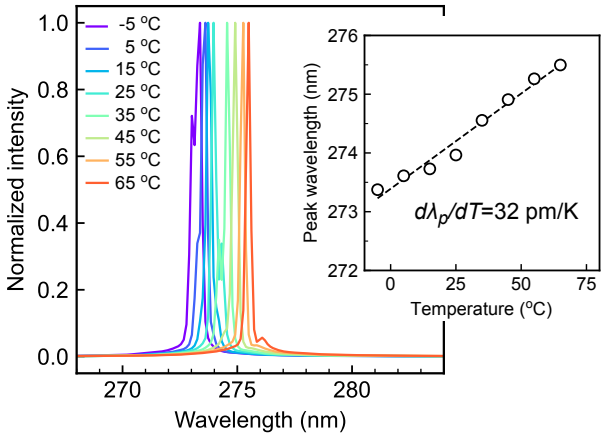

FIG. 3. Normalized edge emission spectra at $1.1 \times I_{th,p}$ for various temperatures. The inset shows the peak shift with the temperature.

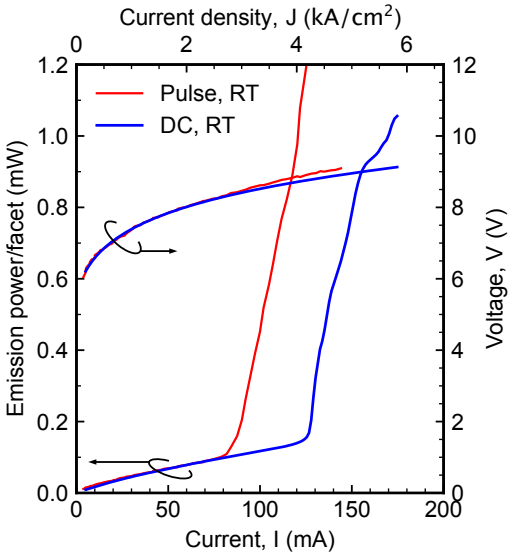

FIG. 4. L–I–V characterisitcs of fabricated UV-C LD under pulsed and DC operations at room temperature.

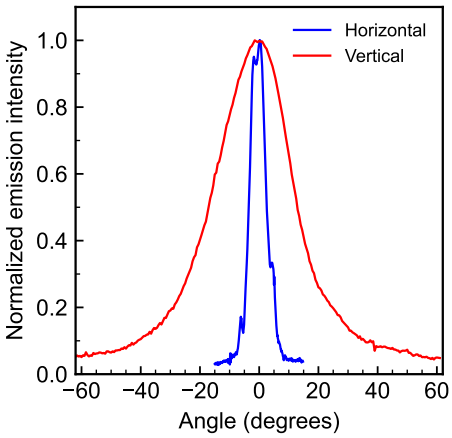

FIG. 5. Measured horizontal and vertical FFPs at emission power of 1 mW

of the horizontal and vertical FFPs were 6 and 30°, respectively. The kinks that appear in the L–I properties are probably due to mode hopping as the current is increased, considering the clearly multiple transverse modes seen in the horizontal FFP. It is expected that the linearity of L–I characteristics above threshold current will be improved by reducing the number of allowed transverse modes, for instance, by using a narrower ridge and gain geometry[12], or by eliminating higher-order modes by employing absorbing layers[13,14]. Reducing the temperature variation due to drive current may also be effective[15].

The I–V curves shown in Fig. 2 are well fitted by $V = V_{on} + IR_s$ when the turn-on voltage V_{on} of the diode is 7.8 V at room temperature and have a temperature dependence of $-13\,\mathrm{mV/K}$ while R_s is nearly constant. This unusual temperature stability of R_s appears to be a contribution of using the p-DPD cladding layer without intentional impurity doping. Much higher temperature dependences of R_s are commonly seen in InGaN-based blue laser diodes where Mg dopants are used for p-cladding layer[16,17]. In these cases, the temperature dependence of R_s is dominated by the large activation energy of Mg dopant in the p-cladding layer. The impact of Si doping on the n-cladding layer conductivity is expected to be much less since the dopant activation energy of Si in $Al_xGa_{1-x}N$ alloys is comparable to the energy of room temperature for Al compositions x up to 0.8[18]. The measured lasing peak shift is reasonably well explained by the temperature dependence of the bandgap energy $E_g(T)$ given by a thermal bandgap narrowing model. The bandgap energy follows the unbroadened Varshini formula

$$E_g(T) = E_g(0) - \frac{\alpha T^2}{\beta + T}$$

and the $\alpha(x)$ and $\beta(x)$ provided by Nepal et al.[19] For an Al composition of $x = 0.53$ for the $Al_xGa_{1-x}N$ quantum well layer, the derived bandgap temperature dependence of $-0.49\,\mathrm{meV/K}$ is in excellent agreement with the measured lasing peak shift that corresponds to $-0.53\,\mathrm{meV/K}$. The difference between the threshold current required for CW operation ($I_{th,c}$) and that for pulsed operation ($I_{th,p}$) can now be understood as being due to the difference in LD junction temperature when the LD is operated under short pulses and low duty cycle, as opposed to the junction temperature under CW operation. Using T_0 of 70 K in Eq. 1, the increase in threshold current from $I_{th,p} = 85\,\mathrm{mA}$ to $I_{th,c} = 125\,\mathrm{mA}$ corresponds to an increase in junction temperature by 27 K. Independently, the thermal resistance θ between the LD juction and the cooling stage (which is dominated by thermal transport through the TO-CAN package) was measured to be $25\,\mathrm{K/W}$ by a standard transient measurement technique[20]. Since the threshold power required to operate the LD CW at room temperature is 1.1 W, given that $V_{th,c} = 8.7\,\mathrm{V}$ and $I_{th,c} = 125\,\mathrm{mA}$, the LD junction temperature under CW operation will be 28 K higher than the LD junction temperature when operated with short pulses and low duty cycle because of the self-heating of the LD chip ($\Delta T = \theta V_{th,c} I_{th,c}$). This temperature difference ΔT is indeed consistent with the increased threshold current required. Note that the power conversion efficiency can be ignored in this calculation since the optical output power is much lower than the input power in the current devices[9].

This self-heating of the junction under CW operation sets a limit on how high $I_{th,p}$ can be while still achieving CW lasing. If the required threshold power rises too rapidly in response to a change in junction temperature, lasing will not be possible. Thus,

$$\theta \frac{d}{dT}\left(V_{th,c} I_{th,c}\right) = \theta \frac{d}{dT}\left(\left(R_s I_{th,c} + V_{on}\right) I_{th,c}\right) < 1$$

must be met. Since $I_{th,c}$ also follows Eq. 1, CW lasing then requires

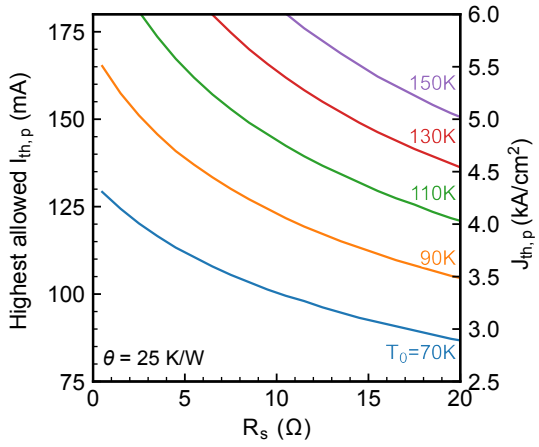

FIG. 6. Calculated highest allowed $I_{th,p}$ under pulsed and low duty operations to realize room-temperature CW lasing in dependence of R_s and T_0.

$$\frac{\theta}{T_o}\left(2R_s{I_{th,c}}^2 + V_{on}I_{th,c}\right) < 1. \quad (2)$$

Equation 2 indicates the importance of decreasing θ and R_s as well as increasing T_0 to achieve CW lasing. Using Eq. 2, the highest allowed $I_{th,c}$ to achieve CW lasing can be determined. Subsequently, the highest allowed $I_{th,p}^{RT}$ (threshold current under pulsed operation at room-temperature) and ΔT can be fixed using Eq. 1 again. Using this approach, one can quantify the contribution of R_s and T_0 on the highest allowed $I_{th,p}^{RT}$. Figure 6 shows the numerically determined results. Approaching the limits shown in Fig. 6 will result in the laser diode junction temperature increasing too rapidly with increasing current under CW operation and, thus, will not allow CW lasing because it will not be possible to achieve the required threshold current.

Plugging in values of present UV-C LD; 25 K/W, 70 K, 7.8 V, and 8.4 Ω for θ, T_0, V_{on}, and R_s, respectively, reveals that the pulsed operation threshold current must be less than 105 mA (3.5 kA/cm^2). Although this condition was achieved in the present work so that room-temperature CW operation could be demonstrated, it is very close to the theoretical limit and indicates the critical importance of the reduction in R_s in the present diode compared that reported in prior work, 12 Ω[9]. As can be seen from Fig. 6, increasing the characteristic temperature T_0 will also ease the thresholding limitation and allow the laser diode to operate at higher temperatures. The T_0 measured here is still significantly lower than the values reported in InGaN-based LDs, which typically exceed 150 K[21,22]. Temperature-dependent mechanisms, such as the broadening of the gain spectrum (decreasing the gain), thermally activated carrier escape, free-carrier absorption, and Auger recombination, may all play a role in decreasing T_0[23–25]. Further improvements in device performance may be achieved through an improved understanding of how device design, material growth, and device fabrication affect T_0.

Here, the room-temperature CW operation of UV-C LDs grown pseudomorphically on AlN substrates was demonstrated for the first time. This key milestone was only possible because of a reduction in the threshold power (1.1 W) required for lasing through reductions of both the threshold voltage (8.7 V) and the threshold current (125 mA). Although UV-C LDs have been demonstrated in prior work, CW lasing was not possible without cooling. The characterization of the temperature dependence of key LD parameters shows that the threshold current for lasing has a strong temperature dependence with a characteristic temperature of 70 K. This strong temperature dependence makes the LD sensitive to self-heating during CW operation even when it endorved with good thermal conductivity of 25 K/W. A reduction in threshold voltage was achieved by reducing the lateral distance between the n- and p-electrodes by tapering the sides of the LD mesa. Past improvements of other nitride-semiconductor LDs indicate the likelyhood that increasing the characteristic temperature is possible and that this improvement will coincide with the improvement of other key LD performance characteristics.

ACKNOWLEDGMENTS

The authors would like to thank Professor Yoshio Honda of Nagoya University and Mr. Kazuhiro Nagase, Dr. Masato Toita and Dr. Naohiro Kuze of Asahi Kasei Corporation for invaluable discussion and considerable support. The authors would like to acknowledge the support of the Center for Integrated Research of Future Electronics, Transformative Electronics Facilities (C-TEFs) of Nagoya University through the use of their facilities for device fabrication. This work was supported by JSPS KAKENHI Grant Number 21H04560.

[1] I. J. Bigio and J. R. Mourant, "Ultraviolet and visible spectroscopies for tissue diagnostics: Fluorescence spectroscopy and elastic-scattering spectroscopy," Physics in Medicine and Biology **42**, 803–814 (1997).
[2] E. B. Hanlon, R. Manoharan, T.-W. Koo, K. E. Shafer, J. T. Motz, M. Fitzmaurice, J. R. Kramer, I. Itzkan, R. R. Dasari, and M. S. Feld, "Prospects for *in vivo* Raman spectroscopy," Physics in Medicine and Biology **45**, R1–R59 (2000).
[3] E. V. Efremov, F. Ariese, and C. Gooijer, "Achievements in resonance Raman spectroscopy," Analytica Chimica Acta **606**, 119–134 (2008).
[4] K. L. Gares, K. T. Hufziger, S. V. Bykov, and S. A. Asher, "Review of explosive detection methodologies and the emergence of standoff deep UV resonance Raman," Journal of Raman Spectroscopy **47**, 124–141 (2016).
[5] A. N. Samant and N. B. Dahotre, "Laser machining of structural ceramics—A review," Journal of the European Ceramic Society **29**, 969–993 (2009).
[6] M. Fujita, H. Ohkawa, T. Somekawa, M. Otsuka, Y. Maeda, T. Matsutani, and N. Miyanaga, "Wavelength and Pulsewidth Dependences of Laser Processing of CFRP," Physics Procedia **83**, 1031–1036 (2016).
[7] S. Ambardar, M. C. Howell, K. Mayilsamy, A. McGill, R. Green, S. Mohapatra, D. V. Voronine, and S. S. Mohapatra, "Ultrafast-UV laser integrating cavity device for inactivation of SARS-CoV-2 and other viruses," Scientific Reports **12**, 11935 (2022).
[8] Z. Zhang, M. Kushimoto, T. Sakai, N. Sugiyama, L. J. Schowalter, C. Sasaoka, and H. Amano, "A 271.8 nm deep-ultraviolet laser diode for room temperature operation," Applied Physics Express **12**, 124003 (2019).
[9] Z. Zhang, M. Kushimoto, A. Yoshikawa, K. Aoto, L. J. Schowalter, C. Sasaoka, and H. Amano, "Continuous-wave lasing of AlGaN-based

ultraviolet laser diode at 274.8 nm by current injection," Applied Physics Express **15**, 041007 (2022).

[10]R. T. Bondokov, S. P. Branagan, N. Ishigami, J. Grandusky, T. Nagatomi, K. Tatsuta, T. Miebach, and J. J. Chen, "Two-Inch Aluminum Nitride (AIN) Single Crystal Growth for Commercial Applications," ECS Transactions **104**, 37–48 (2021).

[11]M. Kushimoto, Z. Zhang, N. Sugiyama, Y. Honda, L. J. Schowalter, C. Sasaoka, and H. Amano, "Impact of heat treatment process on threshold current density in AlGaN-based deep-ultraviolet laser diodes on AlN substrate," Applied Physics Express **14**, 051003 (2021).

[12]M. Yuda, T. Hirono, A. Kozen, and C. Amano, "Improvement of kink-free output power by using highly resistive regions in both sides of the ridge stripe for 980-nm laser diodes," IEEE Journal of Quantum Electronics **40**, 1203–1207 (2004).

[13]T. Tojyo, S. Uchida, T. Mizuno, T. Asano, M. Takeya, T. Hino, S. Kijima, S. Goto, Y. Yabuki, and M. Ikeda, "High-Power AlGaInN Laser Diodes with High Kink Level and Low Relative Intensity Noise," Japanese Journal of Applied Physics **41**, 1829–1833 (2002).

[14]M. Buda, H. Tan, L. Fu, L. Josyula, and C. Jagadish, "Improvement of the kink-free operation in ridge-waveguide laser diodes due to coupling of the optical field to the metal layers outside the ridge," IEEE Photonics Technology Letters **15**, 1686–1688 (2003).

[15]T. Asano, T. Tojyo, T. Mizuno, M. Takeya, S. Ikeda, K. Shibuya, T. Hino, S. Uchida, and M. Ikeda, "100-mW kink-free blue-violet laser diodes with low aspect ratio," IEEE Journal of Quantum Electronics **39**, 135–140 (2003).

[16]H.-Y. Ryu, K.-H. Ha, J.-H. Chae, O.-H. Nam, and Y.-J. Park, "Measurement of junction temperature in GaN-based laser diodes using voltage-temperature characteristics," Applied Physics Letters **87**, 093506 (2005).

[17]M. X. Feng, S. M. Zhang, D. S. Jiang, J. P. Liu, H. Wang, C. Zeng, Z. C. Li, H. B. Wang, F. Wang, and H. Yang, "Thermal characterization of GaN-based laser diodes by forward-voltage method," Journal of Applied Physics **111**, 094513 (2012).

[18]R. Collazo, S. Mita, J. Xie, A. Rice, J. Tweedie, R. Dalmau, and Z. Sitar, "Progress on n-type doping of AlGaN alloys on AlN single crystal substrates for UV optoelectronic applications," physica status solidi (c) **8**, 2031–2033 (2011).

[19]N. Nepal, J. Li, M. L. Nakarmi, J. Y. Lin, and H. X. Jiang, "Temperature and compositional dependence of the energy band gap of AlGaN alloys," Applied Physics Letters **87**, 242104 (2005).

[20]O. Steffens, P. Szabo, M. Lenz, and G. Farkas, "Thermal transient characterization methodology for single-chip and stacked structures," in *Semiconductor Thermal Measurement and Management IEEE Twenty First Annual IEEE Symposium, 2005.* (IEEE, San Jose, CA, USA, 2005) pp. 313–321.

[21]H. Y. Ryu, K. H. Ha, S. N. Lee, T. Jang, H. K. Kim, J. H. Chae, K. S. Kim, K. K. Choi, J. K. Son, H. S. Paek, Y. J. Sung, T. Sakong, O. H. Nam, and Y. J. Park, "Highly stable temperature characteristics of InGaN blue laser diodes," Applied Physics Letters **89**, 031122 (2006).

[22]M. Adachi, Y. Yoshizumi, Y. Enya, T. Kyono, T. Sumitomo, S. Tokuyama, S. Takagi, K. Sumiyoshi, N. Saga, T. Ikegami, M. Ueno, K. Katayama, and T. Nakamura, "Low Threshold Current Density InGaN Based 520–530 nm Green Laser Diodes on Semi-Polar {20\bar21} Free-Standing GaN Substrates," Applied Physics Express **3**, 121001 (2010).

[23]A. Bojarska, J. Goss, Ł. Marona, A. Kafar, S. Stańczyk, I. Makarowa, S. Najda, G. Targowski, T. Suski, and P. Perlin, "Emission wavelength dependence of characteristic temperature of InGaN laser diodes," Applied Physics Letters **103**, 071102 (2013).

[24]B. Galler, P. Drechsel, R. Monnard, P. Rode, P. Stauss, S. Froehlich, W. Bergbauer, M. Binder, M. Sabathil, B. Hahn, and J. Wagner, "Influence of indium content and temperature on Auger-like recombination in InGaN quantum wells grown on (111) silicon substrates," Applied Physics Letters **101**, 131111 (2012).

[25]H.-Y. Ryu, G.-H. Ryu, C. Onwukaeme, and B. Ma, "Temperature dependence of the Auger recombination coefficient in InGaN/GaN multiple-quantum-well light-emitting diodes," Optics Express **28**, 27459 (2020).